Lean NO_x Capture and Reduction by NH_3 via NO^+ Intermediates over H-CHA at Room Temperature

Shunsaku Yasumura,[a] Chong Liu,*[,a,‡] Takashi Toyao,[a,b] Zen Maeno,[a] Ken-ichi Shimizu*[,a,b]

[a] Institute for Catalysis, Hokkaido University, N-21, W-10, Sapporo 001-0021, Japan

[b] Elements Strategy Initiative for Catalysts and Batteries, Kyoto University, Katsura, Kyoto 615-8520, Japan

*Corresponding authors

Chong Liu E-mail: chongliu@cat.hokudai.ac.jp

Ken-ichi Shimizu E-mail: kshimizu@cat.hokudai.ac.jp

‡Present address

State Key Laboratory of Structural Chemistry, Fujian Institute of Research on the Structure of Matter, Chinese Academy of Sciences, Fuzhou, Fujian 350002, China

Keywords:

H-CHA, deNO_x, *in situ* IR spectroscopy, DFT calculation

Abstract

The oxidation of NO to NO_2 and the subsequent reduction by NH_3 via a NO^+ intermediate over a proton-type chabazite zeolite (H-CHA) were investigated by the combination of *in situ* infrared (IR) spectroscopy and density functional theory (DFT) calculations. The *in situ* IR spectral results indicate that the NO^+ species formed under a flow of NO + O_2 at 27–250 °C are more stable at lower temperatures over both H-CHA and copper-cation-exchanged CHA zeolite (Cu-CHA). The Arrhenius plot (T = 27–120 °C) shows a negative apparent activation barrier energy (−11.5 kJ mol^{-1}) for the formation of NO^+ species under the NO + O_2 flow over H-CHA. The time course of the IR spectra at 27 °C shows that NO is oxidized by O_2 to NO_2 and then further converted via N_2O_4 to NO^+ and NO_3^-. The subsequent exposure to NH_3 at 27 °C reduces the NO^+ species to N_2. DFT calculations revealed that Brønsted acid sites in zeolite pores promote the dissociation of N_2O_4 intermediates into NO^+ and NO_3^- species with a low activation barrier (15 kJ mol^{-1}). Moreover, the computed activation barrier for the reduction of NO^+ species by NH_3 was considerably low (6 kJ mol^{-1}). The experimental and theoretical results of this study demonstrate the high potential of Cu-free H-CHA zeolites for promoting the lean NO_x capture to form NO^+ species and the subsequent reduction by NH_3 at room temperature.

1. Introduction

Nitrogen oxides (NO_x), which are harmful acid rain gases, are mainly released from automotive engines, power plants, and chemical industries. The selective catalytic reduction (SCR) of NO_x by NH_3 (NH_3-SCR; Eq.(1)) is widely used to control NO_x emissions from lean exhaust.[1–7]

$$4NO + 4NH_3 + O_2 \rightarrow 4N_2 + 6H_2O \quad (1)$$

Copper-cation-exchanged chabazite (CHA) zeolites (Cu-CHA) have been utilized as commercial catalysts for NH_3-SCR because of their high activity and hydrothermal stability. Although Eq. (1), the so-called standard SCR, is catalyzed by Cu-CHA in current deNO_x systems, the purification of NO_x still requires an operating temperature above 200 °C. To address this issue, the selective reduction of the NO/NO_2 mixture by NH_3 (fast SCR; Eq. (2)) has been investigated as a catalytic system to decrease the operating temperature.

$$2NO + 2NO_2 + 4NH_3 \rightarrow 4N_2 + 6H_2O \quad (2)$$

However, a temperature of 100–150 °C is still required to reduce NO_x under lean operating conditions.[8–11] In addition, a partial conversion of NO to NO_2 using an upstream diesel oxidation catalyst (DOC) is required to provide co-feeding NO_2 for the SCR system. The next generation NH_3-SCR system working at lower temperatures, ideally room temperature, without NO_2 co-feed is strongly desired.

The nitrosonium cation (NO^+) is the oxidized form of NO and one of the key species of nitrosation processes.[12,13] Previous mechanistic studies of the NH_3-SCR reaction indicated that the NO^+ species formed in zeolite pores play a significant role.[14–16] Szanyi et al. conducted both high magnetic field solid-state (SS) magic angle spinning (MAS) nuclear magnetic resonance (NMR) and IR analyses to characterize the key intermediate in the SCR reaction over Cu-CHA. They suggested that side-on $Cu^+\cdots NO^+$ species are formed by the reduction of Cu^{2+} to Cu^+ by using NO at room temperature:[17,18]

$$Cu^{2+} + NO \rightarrow Cu^+\cdots NO^+$$

The same group showed in a subsequent study that NO^+ formation was not the consequence of the Cu^{2+} reduction by NO.[19] A recent theoretical investigation by Grönbeck et al.[20] suggested a mechanism for the low-temperature NH_3-SCR over Cu-CHA in which the NO-induced Cu^{2+} reduction to Cu^+ and NO^+ proceeded with low activation barriers.

Moreover, previous studies have shown that NO^+ species are formed in Cu-free zeolites under low-temperature NO oxidation conditions.[21,22] Hadjiivanov et al. reported the presence of NO^+ species bound to the negative O^- site of H-ZSM-5 by using labeled O_2 molecules ($^{18}O_2$) and deuterium (D_2).[23] From the *in situ* IR spectra of labeled NO molecules (^{15}NO), it was observed that NO oxidation at low temperatures (−173 °C – RT) generated NO^+ species via N_xO_y species over H-ZSM-5.[24] Szanyi et al. investigated the NO oxidation over Na-Y zeolite[25] and observed that NO^+ is formed after exposure to a flow of NO + O_2 at high O_2 pressure via the following reaction:

$$2NO_2 \leftrightarrow N_2O_4 \leftrightarrow NO^+ + NO^{3-}$$

Although previous reports suggest the use of Cu-free zeolites to capture NO as NO^+ at low temperatures, under lean conditions, and without NO_2 addition, the possible role of Cu^{2+} sites forming NO^+ species under NH_3-SCR conditions over Cu-CHA is still debatable.

It is well known that the catalyst-free NO oxidation in the gas phase is faster at lower temperatures and shows a negative activation energy for the NO_2 production.[26] Recently, it was reported that NO oxidation was effectively promoted at low temperatures by both H- and Na-CHA zeolites, showing higher reaction rates than the gas phase reaction.[27,28] Lobo et al. investigated the role of micropores on NO oxidation to NO_2 in the temperature range of 0–150 °C using porous materials such as H-CHA to elucidate the effect of pore size on the reaction.[27,28] It was confirmed that lower temperature facilitated higher NO oxidation rates over H-CHA. Their detailed kinetic study showed a negative apparent activation barrier for NO oxidation caused by the physical confinement effects of the micropores. A subsequent theoretical study compared NO oxidation pathways in the gas phase with that in the cage of CHA. The enthalpic stabilization of the transition states (TS) caused by the confinement effect resulted in a lower free energy.[29]

Based on these reports, it was hypothesized that room-temperature oxidation of NO in H-CHA generates adsorbed NO^+ species as an intermediate via NO_2 disproportionation. In the present study, *in situ* IR spectral measurements were conducted to investigate the produced N_xO_y intermediates during NO oxidation at low temperatures over H-CHA. The outlet gas was simultaneously monitored. In the initial stage of the process, more specifically at 27 °C, NO^+, NO_3^-, and N_2O_4 species were formed over H-CHA. The reduction of the formed NO^+ species with NH_3 was further investigated, demonstrating that the NO^+ species formed were successfully reduced by NH_3 even at 27 °C. Theoretical investigations revealed that the Brønsted acid site (BAS) in H-CHA serves as the active site to convert N_2O_4 intermediates to NO^+ and NO_3^- species with a low activation barrier. Although the proposed reaction that occurs at low temperature over H-CHA zeolite is not catalytic and not directly applicable to steady state NH_3-SCR, understanding the detailed mechanism of this process would be of great importance for real-world applications because most of the emissions from the engine are emitted during the cold start period (i.e., the period before the catalysts are functional[30,31]) and BAS are always present even in the Cu-zeolites. In addition, effective use of this process, together with other non-catalytic approaches such as a passive NOx adsorber system[32], would enable to reduce NOx emissions during the cold start period.

2. Experimental and theoretical methodology

2.1 *In situ* IR

The proton-type CHA zeolite (H-CHA) was obtained by calcining the CHA zeolite (Tosoh, NH_4^+-type, SiO_2/Al_2O_3 = 12.8) at 600 °C for 3 h in air. The Cu-CHA catalysts were prepared by stirring NH_4-type CHA in an aqueous copper acetate solution at room temperature for 3 h, followed by washing with water, drying at 100 °C for 12 h, and calcining at 600 °C for 3 h. The Cu/Al ratio (0.42) of the zeolites was determined by X-ray fluorescence spectroscopy (Shimadzu, EDX-700HS). *In situ* IR spectra were collected in transmission mode using a JASCO FT/IR-4200 spectrometer equipped with a triglycine sulfate (TGS) detector. A quartz IR cell was placed in the spectrometer and connected to a conventional flow reaction system (total flow: 100 mL min^{-1}). The sample was pelletized into a 40 mg self-supported disk and placed in a quartz IR cell with CaF_2 windows. IR spectra were recorded in the transmission mode by accumulating 20 scans at a resolution of 4 cm^{-1}. The reference spectrum of the sample disk was collected under a He flow at the temperature of the measurement. The gas line from the IR cell was directly connected to a homemade gas cell equipped with CaF_2 windows to monitor the generated gases (NO and NO_2) using a JASCO FT/IR-4600 spectrometer (equipped with a TGS detector). To monitor the outlet gases including N_2, H_2O, and NH_3, a mass spectrometer (BELMass, MicrotracBEL Corp.) was utilized. The sample disk was pretreated with 10% O_2 at 500 °C prior to exposure to a flow of 0.1% NO + 10% O_2 at 27 °C. The IR measurement and exposure started simultaneously.

2.2 Computational methods

Density functional theory (DFT) calculations were performed using the Vienna Ab initio Simulation Package (VASP).[33–35] The Perdew–Burke–Ernzerhof (PBE) functional[36] was used together with the projector augmented wave (PAW) method.[37,38] The plane-wave energy cutoff was set to 500 eV. The Brillouin zone sampling was restricted to the Γ point.[39] The dispersion-corrected DFT-D3 (BJ) method was used to describe the van der Waals interactions.[40] Geometry convergence was assumed with a force below 0.05 eV $Å^{-1}$ on each atom. The climbing image nudged elastic band (CI-NEB) method was used to determine the transition state (TS) along with the minimum-energy reaction path.[41]

The unconfined free-state NO_2 was optimized within a large cubic cell (a = b = c = 20 Å), and spin-polarized calculations were applied to account for its unpaired electron. The CHA zeolite was modeled with a 36T unit cell.[42] Chabazite contains a single T site, and one of the lattice Si in the unit cell was substituted by an Al atom to introduce a charge-compensating proton ($H^+O_Z^-$) as the Brønsted acid site (BAS) (Figure 1). Then, full geometry optimizations of the zeolite framework atoms and guest molecules were performed with fixed lattice parameters (a = b = 13.74 Å, c = 14.84 Å; α = β = 90°, γ = 120°).

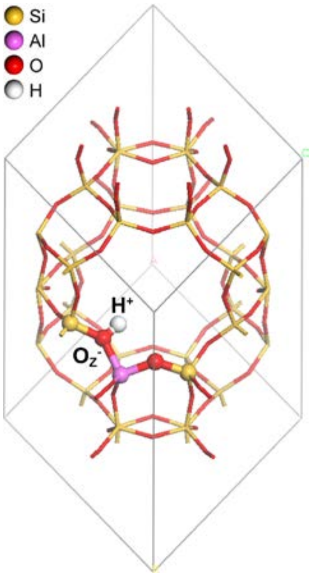

Figure 1. Computational H-CHA zeolite model employed in DFT calculations. The BAS (represented by $H^+O_Z^-$) was introduced as charge-compensating cation by the isomorphous substitution of an Al atom for one lattice Si in the unit cell.

3. Results and discussion

3.1 Room temperature NO oxidation monitored by *in situ* IR spectroscopy

In situ IR spectroscopy was carried out to characterize the generated surface species during NO oxidation at low temperatures. The collected spectra and time course of the heights of the selected IR peaks and the NO and NO_2 concentrations in the outlet gas are shown in Figure 2. In the initial stage, a rapid increase in the intensity of the band at 2166 cm^{-1}, assigned to NO^+ species, was observed.[23–25,43,44] Subsequently, five other IR bands attributed to NO^+NO_2,[25,43] N_2O_4,[24,25,44,45] adsorbed HNO_3 (HNO_{3ad}),[43–45] and nitrate species (NO_3^-)[24,25,43,44] appeared at 2220, 1750, 1666, and 1380 cm^{-1}, respectively. NO_3^- species, which were observed by the IR measurements, were produced by some side-reactions such as the dissociation of HNO_3 and N_2O_4 that give H^+–NO_3^- and NO^+–NO_3^- species, respectively.[46] After 400 s of exposure, the formation of NO^+, HNO_{3ad}, and N_2O_4 was saturated, and the concentration of NO_2 in the outlet gas started to increase in spite of the unchanged NO concentration. In addition, the NO^+ peak height decreased after saturation occurred because of the subsequent formation of NO^+NO_2 species. In addition to the proposals in previous reports,[24,25,47,48] these results indicate that NO oxidation in the micropores of H-CHA generates NO_2, which is then transformed to NO^+ and HNO_3 on the BAS via the N_2O_4 intermediate.

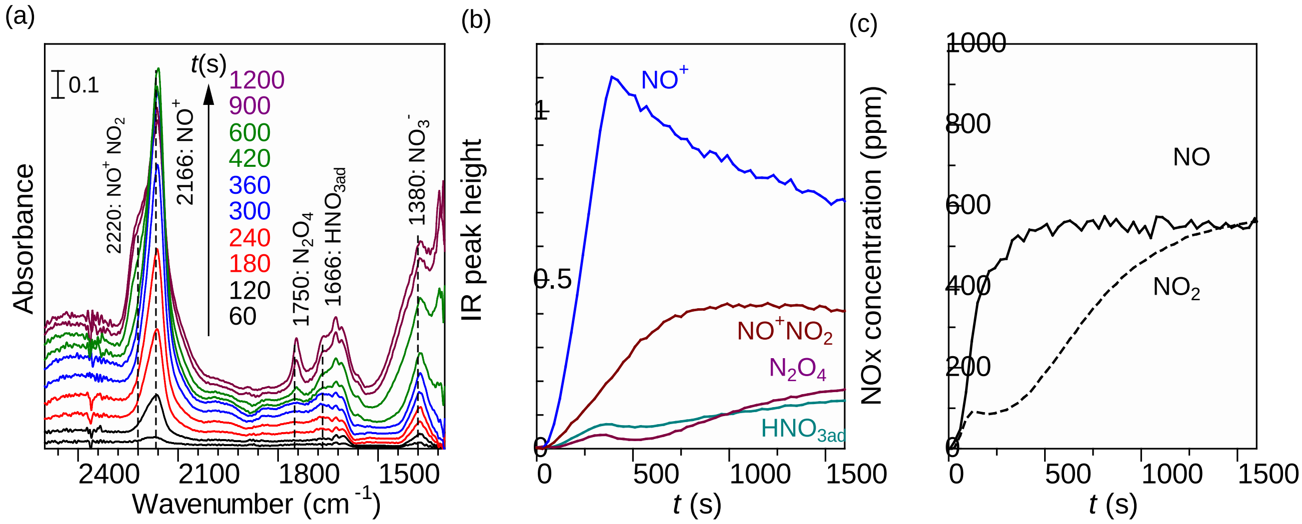

Figure 2. (a) *In situ* IR spectra of species adsorbed on H-CHA (40 mg) under a flow of 0.1% NO + 10% O_2 at 27 °C (total flow: 100 ml min^{-1}). (b) Time dependence of the IR peak height for surface species and (c) the concentration of NO and NO_2 in outlet gas monitored by a gas cell.

As mentioned in the introduction, the role of Cu sites on the formation and adsorption of NO^+ in Cu-CHA is still controversial.[17,18,49] To identify the adsorption site for NO^+ species, Figure 3 presents the IR spectra of H-CHA (Figure 3a) and Cu-CHA (Figure 3c) at several temperatures (27–250 °C) after exposure to a flow of NO + O_2. Using H-CHA, IR bands corresponding to NO^+ and NO_3^- species were observed at 2166 cm^{-1} and 1626 cm^{-1}, respectively.[19,23,50] In the case of Cu-CHA, IR bands related to NO_3^- species adsorbed on Cu^{2+} cations (Cu^{2+}-NO_3^- species) were observed at 1626 cm^{-1}, 1600 cm^{-1}, and 1570 cm^{-1}, respectively, in addition to NO^+ species at 2160 cm^{-1}.[19,50–52] The temperature dependence of the IR peak heights is shown in Figure 3b,d. Over both zeolites, NO^+ species decreased with increasing temperature and were hardly observed at temperatures higher than 250 °C, indicating that a lower temperature favors the formation of NO^+ species. The comparison of the IR peak heights between H-CHA and Cu-CHA indicated that the Cu sites in Cu-CHA do not play a better role in the formation of NO^+ in the low-temperature region than the BAS in H-CHA.

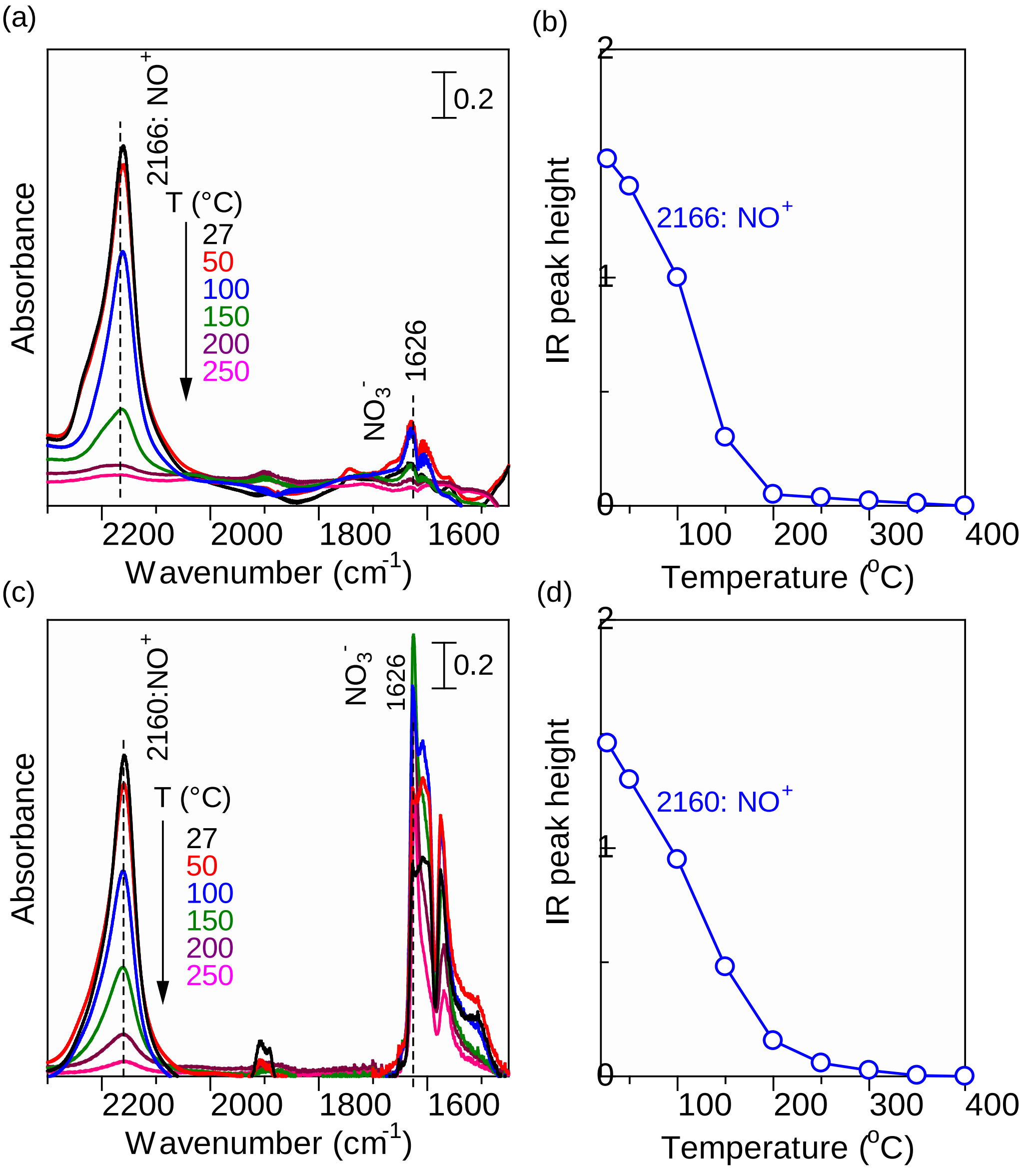

Figure 3. IR spectra of NO^+ intermediate under a flow of 0.1% NO + 10% O_2 at varying temperatures (27–250 °C) over (a) H-CHA and (c) Cu-CHA; temperature-dependent IR peak heights of NO^+ species over (b) H-CHA and (d) Cu-CHA.

3.2 Kinetic study of NO^+ formation

IR spectra of the adsorbed N_xO_y species on H-CHA were collected in the low-temperature region (27–120 °C) under a flow of 0.1% NO + 10% O_2. The IR spectra collected over time at different temperatures are provided in Figure S1. The reaction rates for NO^+ formation under a flow of NO + O_2 were evaluated using the initial slope of the evolution of the IR peak area corresponding to NO^+ species.

The Arrhenius plot (Figure 4a) shows a linear slope in the applied temperature range, resulting in an apparent activation energy (*E*a) of −11 kJ mol^{-1}. This indicates that a lower temperature kinetically favors the NO^+ formation over H-CHA. Lobo et al. reported the *E*a for the overall NO_2 formation, which is described as follows:[28]

$$2NO + O_2 \rightarrow 2NO_2 \quad (5)$$

The reported *E*a value for H-CHA is also negative (−37.5 kJ mol^{-1}) in the temperature range of 70–150 °C, which indicates that the oxidation of NO to NO_2 over H-CHA is faster at lower temperatures.

The dependencies of the NO^+ formation rates on O_2 (p_{O2}, 0.1–10%, Figure 4b) and NO pressure (p_{NO}, 0.01–1%, Figure 4c) were determined (IR spectra can be found in the Figure S2). The reaction orders of O_2 (0.35) and NO (0.63) for the NO^+ formation using NO oxidation over H-CHA were both positive. Lobo et al. reported that the reaction orders of p_{O2} (1.03) and p_{NO} (2.04) for the NO oxidation to NO_2 over H-CHA were positive.[28] As discussed before, the potential mechanism for the formation of NO^+ over H-CHA involves the N_2O_4 intermediate, resulting from the NO_2 dimerization (Eq. (6)) and its subsequent decomposition (Eq. (7)).

$$2NO_2 \rightleftharpoons N_2O_4 \quad (6)$$

$$N_2O_4 + H^+O_Z^- \rightarrow NO^+O_Z^- + HNO_3 \quad (7)$$

These reactions do not include O_2 and NO, while the reaction orders of O_2 and NO for the formation of NO^+ species are positive. This suggests that the NO oxidation to NO_2 is slower than the subsequent dimerization into the N_2O_4 intermediate as well as its decomposition to NO^+ and HNO_3. This interpretation is also consistent with the negative *E*a value for NO^+ formation (Figure 4a).

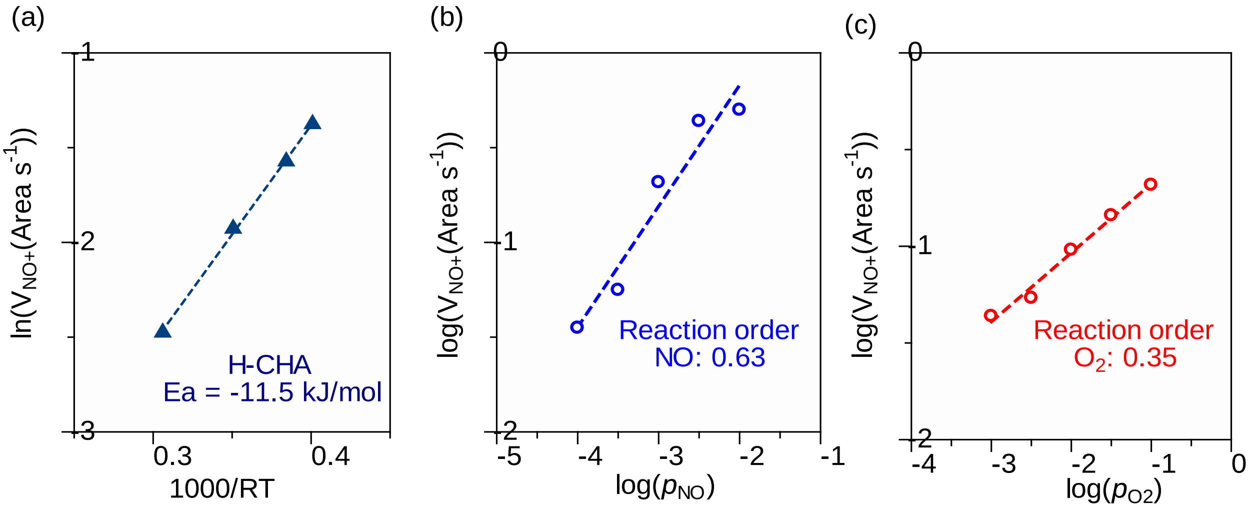

Figure 4. (a) Arrhenius plots for NO^+ formation over H-CHA zeolites in the low-temperature regime (27–120 °C). The NO^+ formation rate was obtained from the evolution of its IR peak area. Log-log plot of the reaction rate of NO^+ formation at 40 °C vs (b) NO pressure (at 10% O_2) and (c) O_2 pressure (at 0.1% NO).

3.3 Room temperature reduction of NO^+ with NH_3

In the previous sections, it was demonstrated that a lower temperature favors the NO oxidation and the sequential NO^+ formation over H-CHA. In this section, the reduction of NO^+ species with NH_3 was investigated using *in situ* IR spectroscopy combined with gas phase analysis by mass spectroscopy (MS). The IR disk of H-CHA was first subjected to a flow of 0.1% NO + 10% O_2 for 15 min, followed by purging with He for 6 min. Then, a flow of 0.1% NH_3 was introduced into the *in situ* IR cell, while monitoring the outlet gas components (N_2, H_2O, and NH_3) by MS. Once the He flow was switched to NH_3/He, the IR spectra were measured (Figure 5a). After being subjected to NH_3 for 100 s, the IR peak at 2166 cm^{-1} corresponding to NO^+ species decreased and another IR band at 1455 cm^{-1} related to NH_3 adsorbed on the BAS (NH_4^+ on zeolite oxygen, denoted as B-NH_3) appeared.[53] With further exposure, NO^+ species decreased and were rarely observed after 2000 s (Figure S3). Figure 5b shows the evolution of the MS peaks for N_2, H_2O, and NH_3 in the outlet gas as well as the consumption rates of NO^+ species estimated by the numerical differentiation of the evolution of the IR peak. The IR results show that the NO^+ consumption rate nearly coincides with the N_2 formation rate.

The initial step in the NO^+ reduction with NH_3 is the formation of a nitrosamide (H_2NNO) intermediate[54,55]:

$$NO^+O_Z^- + NH_3 \rightarrow H_2NNO + H^+O_Z^- \quad (8)$$

The H_2NNO intermediate is thermally decomposed to N_2 and H_2O:

$$H_2NNO \rightarrow N_2 + H_2O \quad (9)$$

The more detailed mechanism is discussed in the following theoretical investigation.

The experimental results showed that H-CHA successfully promoted the conversion of NO + O_2 to the NO^+ intermediate, which is then reduced by NH_3 at room temperature to N_2.

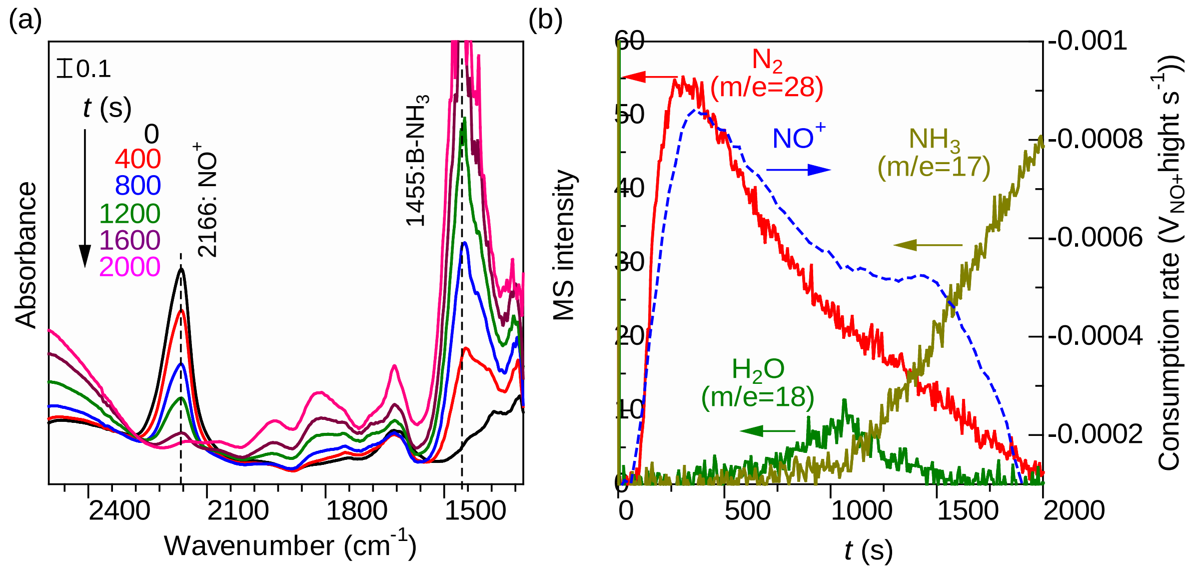

Figure 5. (a) *In situ* IR spectra of species adsorbed at 27 °C under a flow of 0.1% NH_3 on H-CHA pre-exposed to a flow of 0.1% NO + 10% O_2. (b) The consumption rate of NO^+ species corresponding to the IR peak height and MS intensities of N_2, H_2O, and NH_3.

3.4 Theoretical investigation into the formation and reduction of NO^+ over H-CHA

To better understand the formation of NO^+ species and their reactivity toward the production of N_2, DFT calculations were conducted to unravel the detailed reaction mechanism. The H-CHA zeolite was simulated using a periodic 36T cell (Figure 1). The reaction of two NO_2 molecules over the BAS in H-CHA to produce NO^+ species was first investigated. As discussed in previous studies,[47,56,57] in many instances, NO_2 participates in chemical reactions via its dimer form (N_2O_4 species) rather than the NO_2 monomer. NO_2 dimers exist in different forms, such as symmetric N_2O_4, *cis*-ONO-NO_2, and *trans*-ONO-NO_2. Computational results on gas-phase[47] and zeolite-confined systems[54,55] suggested that *trans*-ONO-NO_2 acts as the precursor for the ionic separation and subsequent production of NO^+ and NO_3^- ion pairs. Herein, the *trans*-ONO-NO_2 adsorbed on the BAS was also considered for evaluating the production of NO^+ species over H-CHA (Figure 6). Comparing the unconfined *trans*-ONO-NO_2 in the gas phase (Figure 6a) with the confined version in an isostructural siliceous CHA (Figure 6b), the N(1)–O(1) bond length of *trans*-ONO-NO_2 in H-CHA (Figure 6c) is elongated from approximately 1.61 Å to 1.80 Å, suggesting a pre-activation of *trans*-ONO-NO_2 for ionic separation upon the adsorption on the BAS. The following reaction steps for NO^+ production are illustrated in Figure 7. $H^+O_z^-$·*trans*-ONO-NO_2 reacts via TS1 with an activation barrier of 15 kJ mol^{-1}, which produces NO^+ accompanied by a proton transfer from the BAS to NO_3^-, yielding a HNO_3 moiety (NO^+ O_z^-·HNO_3). The zeolite BAS is essential for promoting the ionic separation of *trans*-ONO-NO_2 to produce NO^+ species because the presence of the Brønsted proton (H^+) stabilizes anionic NO_3^-.

The effect of the H-CHA BAS was further assessed by comparing the reaction pathways of *trans*-ONO-NO_2 → NO^+ + NO_3^- in the unconfined gas phase and BAS-free siliceous CHA (Figure 8 and Table 1). For the unconfined gas-phase *trans*-ONO-NO_2 (Figure 8a), the ionic separation to form NO^+ and NO_3^- ion pairs is realized with the gradual elongation of the N(1)–O(1) bond from 1.61 to approximately 4.39 Å, which requires an activation energy as high as 140 kJ mol^{-1}. Similarly, the reaction of *trans*-ONO-NO_2 → NO^+ + NO_3^- over the proton-free siliceous CHA zeolite (Figure 8b) occurs with N(1)–O(1) bond elongation from 1.60 to 6.31 Å. This requires a high activation barrier of 155 kJ mol^{-1} with an endothermicity of 127 kJ mol^{-1}. In contrast, the BAS promoted the dissociation of *trans*-ONO-NO_2 over H-CHA (Figure 8c), which has an activation barrier of only 15 kJ mol^{-1} to produce NO^+ and a HNO_3 moiety (protonated NO_3^-). In this process, the N(1)–O(1) bond is elongated from 1.80 to 2.35 Å. A proton is simultaneously transferred from the BAS to the terminal oxygen (O(2)) in *trans*-ONO-NO_2 (lengthening the distance O_z–H from 1.00 to 1.57 Å and shortening that of O(2)–

H from 1.67 to 1.04 Å). The further isolation of the HNO_3 moiety in $NO^+O_z^-{\cdot}HNO_3$ at a N(1)–O(1) distance of 4.94 Å is disfavored by 42 kJ mol^{-1}, exhibiting an activation energy of 63 kJ mol^{-1}, which is much lower than that for siliceous CHA. The ionic separation of *trans*-ONO-NO_2 to form NO^+ and NO_3^- in the unconfined state or in siliceous CHA is restricted by strong electrostatic interactions, whereas the BAS in H-CHA can promote this process by the protonation of the anionic NO_3^- to compensate for the energy requirement of NO^+ formation. Comparing the results of *trans*-ONO-NO_2 → NO^+ + NO_3^- (Table 1) clearly reveals that the formation of NO^+ species is significantly enhanced by the presence of the BAS.

The reactivity of the NO^+ species was then evaluated by considering its reaction with NH_3 (Figure 9). The NO^+ present at O_z^- sites reacts with the adsorbed NH_3 via TS2 with a low activation barrier energy of only 6 kJ mol^{-1}, which produces H_2NNO and a Brønsted proton that is donated back to the zeolite oxygen site to regenerate the BAS. H_2NNO can subsequently decompose to N_2 and H_2O, and the thermodynamic estimation indicates that this process is strongly exothermic (–219 kJ mol^{-1}). It was previously suggested that the conversion of H_2NNO to N_2 and H_2O occurs via multiple proton transfers catalyzed by the BAS.[15,20,54,55,58–60] A vibrational analysis conducted to estimate the frequency of the NO^+ species located on the negative O_z^- site gave a stretching vibration frequency at 2054 cm^{-1}, which reasonably agrees with the experimental values determined for H-CHA and Cu-CHA (2166 cm^{-1} and 2160 cm^{-1}, respectively) as well as that of a previous report.[61]

The combined results of *in situ* IR spectroscopy and DFT calculations suggest the following mechanism for the low-temperature NO oxidation and sequential NH_3 reduction (Figure 10). First, NO oxidation occurs to form NO_2 at a relatively slow reaction rate. Then, two NO_2 molecules react over the BAS forming *trans*-ONO-NO_2 to produce NO^+ and HNO_3 species (2 $NO_2 \rightarrow N_2O_4 + H^+O_z^- \rightarrow NO^+O_z^- + HNO_3$). The formed $NO^+O_z^-$ species showed high reactivity toward the NH_3 reduction to afford H_2NNO, which subsequently decomposes to N_2 and H_2O ($NO^+O_z^- + NH_3 \rightarrow H^+O_z^- + H_2NNO \rightarrow H^+O_z^- + N_2 + H_2O$). The formed HNO_3 further reacts with NH_3 to form NH_4NO_3 that can decompose at higher temperature.[14] The presence of the BAS in H-CHA was essential for promoting these reactions. In addition, our findings confirm the high potential of the BAS in both H-CHA and Cu-CHA for the promotion of low-temperature SCR reactions although the catalytic applicability of the present system has not yet been verified.

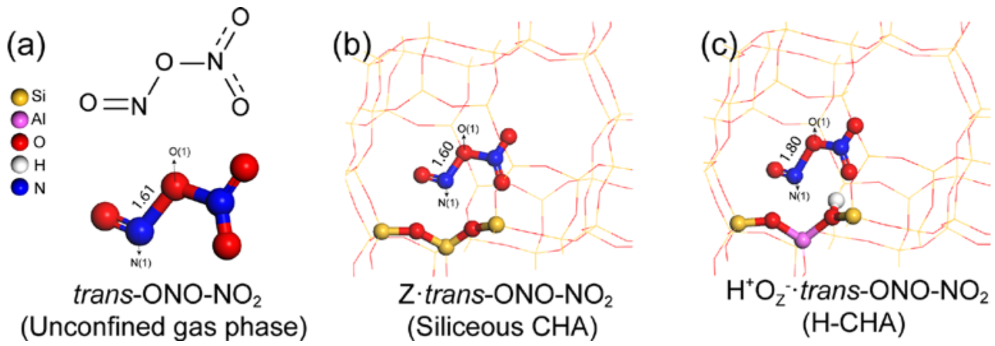

Figure 6. Optimized *trans*-ONO-NO_2 structures in (a) the unconfined gas phase, (b) siliceous CHA, and (c) H-CHA.

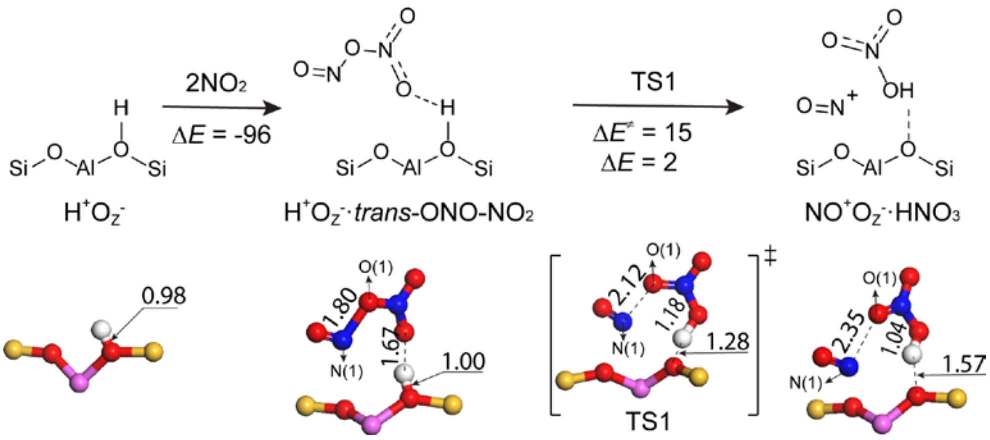

Figure 7. Formation of NO^+ species from two NO_2 molecules over H-CHA. The optimized structures of the corresponding intermediates and transition state are presented at the bottom, and only atoms around the reaction site are shown for clarity. Energies and atomic distances are indicated in kJ mol^{-1} and Å, respectively.

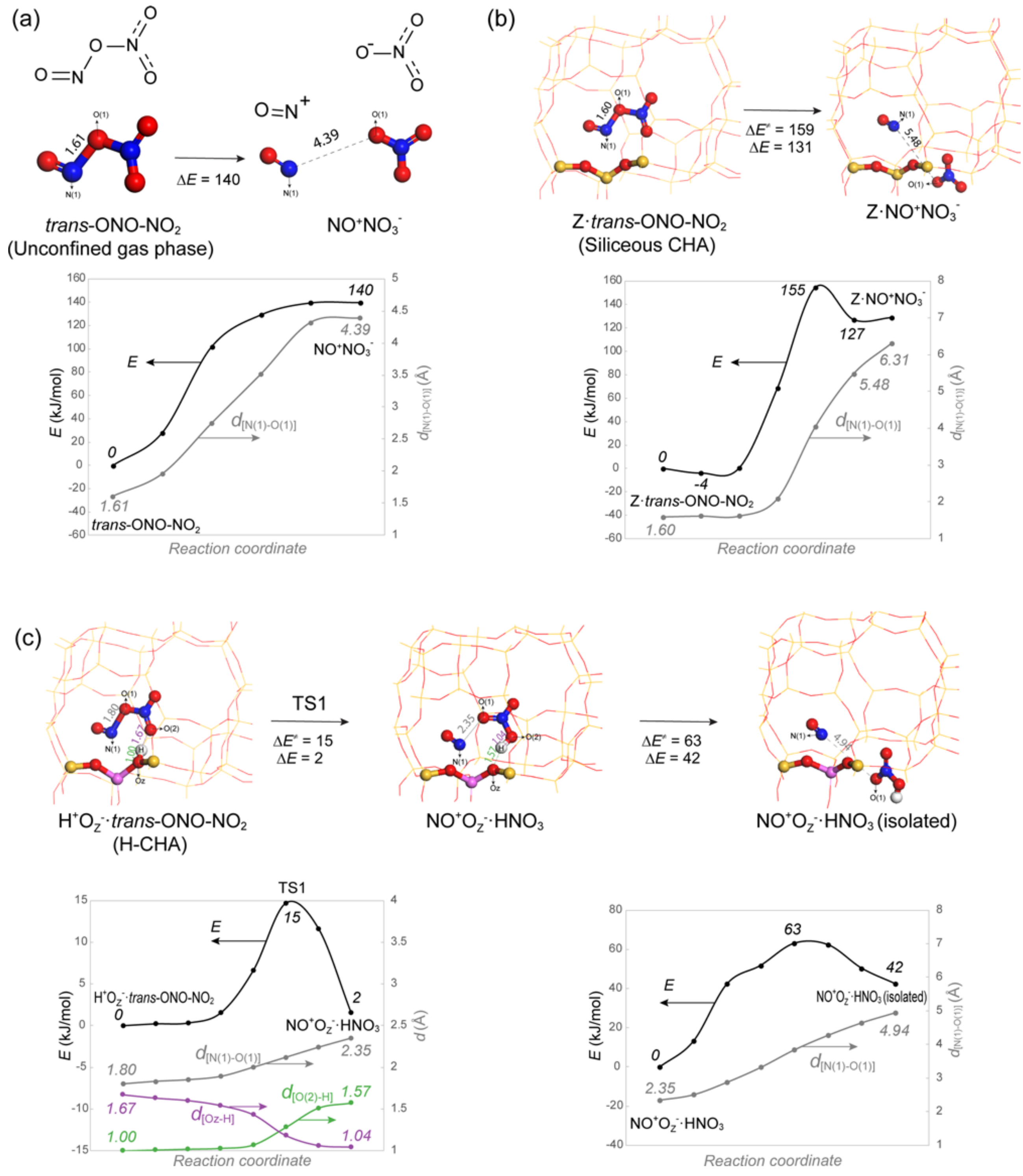

Figure 8. Comparison of *trans*-ONO-NO2 → NO^+ + NO_3^- reaction paths in (a) the unconfined gas phase, (b) siliceous CHA zeolite, and (c) H-CHA. The corresponding plots of CI-NEB calculations to determine the minimum-energy reaction paths are presented at the bottom.

Table 1. Summarized reaction barrier ($\Delta E^{\ddagger}$) and energy change (ΔE) for the reaction of *trans*-ONO-NO_2 → NO^+ + NO_3^- in the unconfined gas phase, siliceous CHA, and H-CHA.

Model	$\Delta E^{\ddagger}$	ΔE
Unconfined gas phase	140	140
Siliceous CHA	155	127
H-CHA	15	2

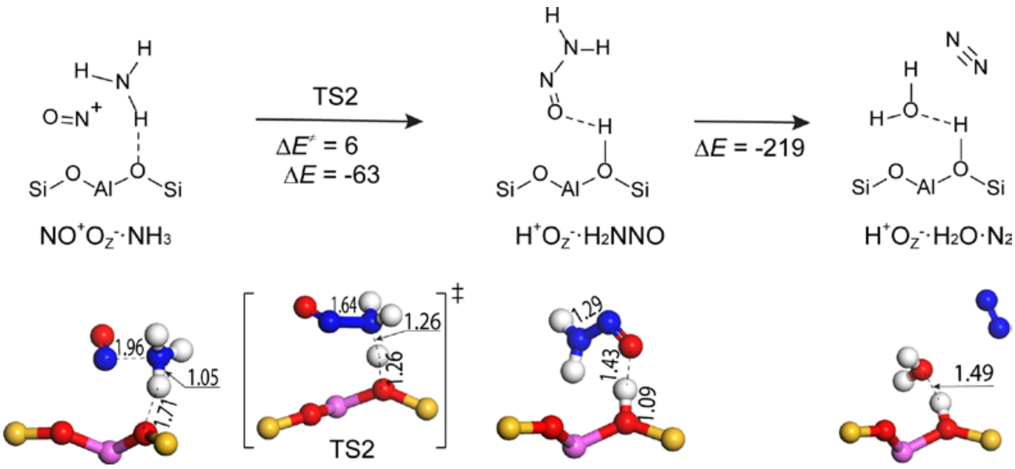

Figure 9. Reaction of NO^+ with NH_3 to produce N_2 and H_2O over H-CHA. The optimized structures of the corresponding intermediates and transition state are displayed at the bottom, and only atoms around the reaction site are shown for clarity. Energies and atomic distances are indicated in kJ mol^{-1} and Å, respectively.

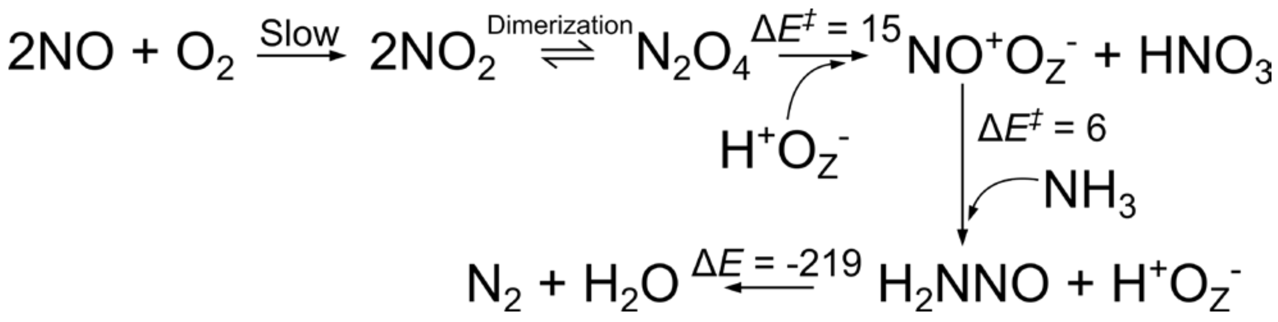

Figure 10. Proposed mechanism of NO oxidation and the following reduction by NH_3 over the zeolite BAS in the low temperature region. (Unit: kJ mol^{-1})

4. Conclusions

The formation of the NO^+ intermediate under lean NOx conditions and its reactivity with NH_3 in H-CHA at room-temperature were studied by *in situ* IR spectroscopy and DFT calculations. In the initial oxidation regime, a rapid increase in NO^+ species was observed at 27 °C under a flow of NO + O_2, while NO_2 generated by NO oxidation was rarely observed in the outlet gas due to its transformation to NO^+ and HNO_3 species via N_2O_4 intermediates. Kinetic studies of the NO^+ formation showed a negative *E*a value (−11 kJ mol^{-1}) and a positive dependence on p_{NO} and p_{O2} (0.63 and 0.35, respectively). Upon exposure to NH_3, NO^+ species were reduced at 27 °C to N_2. DFT calculations indicated the ability of the BAS in H-CHA to pre-activate N_2O_4 species and promote the formation of NO^+ and HNO_3 species with a low activation barrier (15 kJ mol^{-1}). The reaction of NO^+ with NH_3 at O_z^- sites was also theoretically investigated. The formation of the H_2NNO intermediate proceeded with an activation barrier of 6 kJ mol^{-1}, and it subsequently decomposed to N_2 and H_2O, which was a strongly exothermic process (–219 kJ mol^{-1}). The current study revealed that the BAS in CHA zeolite acts as an active site for room-temperature SCR, promoting the NO oxidation and the subsequent reduction process. Although the main catalytically active component in the current diesel emission control system is Cu in the Cu-zeolites, protonic sites as BAS also exist because the commercial Cu-CHA catalysts normally have an ion exchange level of ~60%.[62,63] In addition, most of the emissions are released during the cold start period (typically below 100 °C), and therefore, understanding and controlling the behaviors of both protonic sites and Cu sites in the low-temperature regime would be of vital importance. Our present study suggests that although the proposed process is not catalytic, effective use of protonic sites of the zeolite catalysts, possibly combined with other non-catalytic methods such as a passive NOx adsorber system, could suppress NOx emissions at low temperature.

Associated Content

Supporting Information

The Supporting Information is available free of charge on the ACS Publications website at http://pubs.acs.org.

In situ IR spectra of adsorbed species on H-CHA under different conditions; time course of IR peak height of NO^+ species on H-CHA; geometric parameters (xyz coordinates) of DFT optimized transition states and intermediates

Author Information

Corresponding authors

*E-mail for K.S.:kshimizu@cat.hokudai.ac.jp.

*E-mail for C.L.:chongliu@cat.hokudai.ac.jp.

Conflict of Interest

The authors declare no conflict of interest.

Acknowledgement

This work was financially supported by the JST-CREST project JPMJCR17J3, KAKENHI grants 20H02775, 20H02518, and 17H01341 from JSPS and by the MEXT projects Elements Strategy Initiative (JPMXP0112101003) and IRCCS. This research was one of the projects promoted by the research association of Automotive Internal Combustion Engines (AICE) and was financially supported by the Japan Ministry of Economy, Trade, and Industry. The authors thank the technical division of the Institute for Catalysis (Hokkaido University) for manufacturing the experimental equipment. C.L. acknowledges the JSPS postdoctoral fellowship (No. P19059). The calculations were performed on the supercomputers RIIT (Kyushu University) and ACCMS (Kyoto University).

References

(1) Brandenberger, S.; Kröcher, O.; Tissler, A.; Althoff, R. The State of the Art in Selective Catalytic Reduction of NO_x by Ammonia Using Metal-Exchanged Zeolite Catalysts. *Catal. Rev. - Sci. Eng.* **2008**, *50*, 492–531.

(2) Beale, A. M.; Gao, F.; Lezcano-Gonzalez, I.; Peden, C. H. F.; Szanyi, J. Recent Advances in Automotive Catalysis for NOx Emission Control by Small-Pore Microporous Materials. *Chem. Soc. Rev.* **2015**, *44*, 7371–7405.

(3) Liu, F.; Yu, Y.; He, H. Environmentally-Benign Catalysts for the Selective Catalytic Reduction of NO_x from Diesel Engines: Structure–Activity Relationship and Reaction Mechanism Aspects. *Chem. Commun.* **2014**, *50*, 8445–8463.

(4) Zhang, R.; Liu, N.; Lei, Z.; Chen, B. Selective Transformation of Various Nitrogen-Containing Exhaust Gases toward N2 over Zeolite Catalysts. *Chem. Rev.* **2016**, *116*, 3658–3721.

(5) Priya, S. V.; Ohnishi, T.; Shimada, Y.; Kubota, Y.; Masuda, T.; Nakasaka, Y.; Matsukata, M.; Itabashi, K.; Okubo, T.; Sano, T.; Tsunoji, N.; Yokoi, T.; Ogura, M. A Collective Case Screening of the Zeolites Made in Japan for High Performance NH_3-SCR of NOx. *Bull. Chem. Soc. Jpn.* **2018**, *91*, 355–361.

(6) Marberger, A.; Petrov, A. W.; Steiger, P.; Elsener, M.; Kröcher, O.; Nachtegaal, M.; Ferri, D. Time-Resolved Copper Speciation during Selective Catalytic Reduction of NO on Cu-SSZ-13. *Nat. Catal.* **2018**, *1*, 221–227.

(7) Liu, K.; Yan, Z.; Shan, W.; Shan, Y.; Shi, X.; He, H. Quantitative Determination of the Cu Species, Acid Sites and NH_3-SCR Mechanism on Cu-SSZ-13 and H-SSZ-13 at Low Temperatures. *Catal. Sci. Technol.* **2020**, *10*, 1135–1150.

(8) Shan, Y.; Shi, X.; He, G.; Liu, K.; Yan, Z.; Yu, Y.; He, H. Effects of NO_2 Addition on the NH_3-SCR over Small-Pore Cu-SSZ-13 Zeolites with Varying Cu Loadings. *J. Phys. Chem. C* **2018**, *122*, 25948–25953.

(9) Gramigni, F.; Selleri, T.; Nova, I.; Tronconi, E. Catalyst Systems for Selective Catalytic Reduction + NO_x Trapping: From Fundamental Understanding of the Standard SCR Reaction to Practical Applications for Lean Exhaust after-Treatment. *React. Chem. Eng.* **2019**, *4*, 1165–1178.

(10) Richter, M.; Eckelt, R.; Parlitz, B.; Fricke, R. Low-Temperature Conversion of NO_x to N_2 by Zeolite-Fixed Ammonium Ions. *Appl. Catal. B Environ.* **1998**, *15*, 129–146.

(11) Sanchez-Escribano, V.; Montanari, T.; Busca, G. Low Temperature Selective Catalytic Reduction of NOx by Ammonia over H-ZSM-5: An IR Study. *Appl. Catal. B Environ.* **2005**, *58*, 19–23.

(12) Hughes, M. N. Relationships between Nitric Oxide, Nitroxyl Ion, Nitrosonium Cation and Peroxynitrite. *Biochim. Biophys. Acta - Bioenerg.* **1999**, *1411*, 263–272.

(13) Hadjiivanov, K. I. Identification of Neutral and Charged N_xO_y Surface Species by IR Spectroscopy. *Catal. Rev. - Sci. Eng.* **2000**, *42*, 71–144.

(14) Kubota, H.; Liu, C.; Toyao, T.; Maeno, Z.; Ogura, M.; Nakazawa, N.; Inagaki, S.; Kubota, Y.; Shimizu, K. Formation and Reactions of NH_4NO_3 during Transient and Steady-State NH_3-SCR of NO_x over H-AFX Zeolites: Spectroscopic and Theoretical Studies. *ACS Catal.* **2020**, *10*, 2334–2344.

(15) Li, S.; Zheng, Y.; Gao, F.; Szanyi, J.; Schneider, W. F. Experimental and Computational Interrogation of Fast SCR Mechanism and Active Sites on H-Form SSZ-13. *ACS Catal.* **2017**, *7*, 5087–5096.

(16) Loiland, J. A.; Lobo, R. F. Oxidation of Zeolite Acid Sites in NO/O_2 Mixtures and the Catalytic Properties of the New Site in NO Oxidation. *J. Catal.* **2015**, *325*, 68–78.

(17) Kwak, J. H.; Lee, J. H.; Burton, S. D.; Lipton, A. S.; Peden, C. H. F.; Szanyi, J. A Common Intermediate for N2 Formation in Enzymes and Zeolites: Side-On Cu-Nitrosyl Complexes. *Angew. Chem. Int. Ed.* **2013**, *52*, 9985–9989.

(18) Szanyi, J.; Kwak, J. H.; Zhu, H.; Peden, C. H. F. Characterization of Cu-SSZ-13 NH_3 SCR Catalysts: An in Situ FTIR Study. *Phys. Chem. Chem. Phys.* **2013**, *15*, 2368–2380.

(19) Chen, H. Y.; Kollar, M.; Wei, Z.; Gao, F.; Wang, Y.; Szanyi, J.; Peden, C. H. F. Formation of NO^+ and Its Possible Roles during the Selective Catalytic Reduction of NO_x with NH_3 on Cu-CHA Catalysts. *Catal. Today* **2019**, *320*, 61–71.

(20) Chen, L.; Janssens, T. V. W.; Vennestrøm, P. N. R.; Jansson, J.; Skoglundh, M.; Grönbeck, H. A Complete Multisite Reaction Mechanism for Low-Temperature NH3-SCR over Cu-CHA. *ACS Catal.* **2020**,*10*, 5646–5656.

(21) Bell, A. T. Experimental and Theoretical Studies of NO Decomposition and Reduction over Metal-Exchanged ZSM-5. *Catal. Today* **1997**, *38*, 151–156.

(22) Eng, J.; Bartholomew, C. H. Kinetic and Mechanistic Study of NOx Reduction by NH_3 over H-Form Zeolites I. Kinetic and Mechanistic Insights into NO Reduction over H-ZSM-5. *J. Catal.* **1997**, *171*, 14–26.

(23) Hadjiivanov, K.; Saussey, J.; Freysz, J. L.; Lavalley, J. C. FT-IR Study of NO + O2 Co-Adsorption on H-ZSM-5: Re-Assignment of the 2133 cm^{-1} Band to NO^+ Species. *Catal. Lett.* **1998**, *52*, 103–108.

(24) Penkova, A.; Hadjiivanov, K.; Mihaylov, M.; Daturi, M.; Saussey, J.; Lavalley, J. C. FTIR Spectroscopic Study of Low Temperature NO Adsorption and NO + O_2 Coadsorption on H-ZSM-5. *Langmuir* **2004**, *20*, 5425–5431.

(25) Szanyi, J.; Kwak, J. H.; Moline, R. A.; Peden, C. H. F. The Adsorption of NO_2 and the NO + O_2 Reaction on Na-Y,FAU: An in Situ FTIR Investigation. *Phys. Chem. Chem. Phys.* **2003**, *5*, 4045–4051.

(26) Tsukahara, H.; Ishida, T.; Mayumi, M. Gas-Phase Oxidation of Nitric Oxide: Chemical Kinetics and Rate Constant. *Nitric Oxide* **1999**, *3*, 191–198.

(27) Artioli, N.; Lobo, R. F.; Iglesia, E. Catalysis by Confinement: Enthalpic Stabilization of NO Oxidation Transition States by Micropororous and Mesoporous Siliceous Materials. *J. Phys. Chem. C* **2013**, *117*, 20666–20674.

(28) Loiland, J. A.; Lobo, R. F. Low Temperature Catalytic NO Oxidation over Microporous Materials. *J. Catal.* **2014**, *311*, 412–423.

(29) Maestri, M.; Iglesia, E. First-Principles Theoretical Assessment of Catalysis by Confinement: NO-O2 Reactions within Voids of Molecular Dimensions in Siliceous Crystalline Frameworks. *Phys. Chem. Chem. Phys.* **2018**, *20*, 15725–15735.

(30) Chen, H.-Y.; Liu, D.; Weigert, E.; Cumaranatunge, L.; Camm, K.; Bannon, P.; Cox, J.; Arnold, L. Durability Assessment of Diesel Cold Start Concept (DCSC™) Technologies. *SAE Int. J. Engines* **2017**, *10*.

(31) Lee, J.; Theis, J. R.; Kyriakidou, E. A. Vehicle Emissions Trapping Materials: Successes, Challenges, and the Path Forward. *Appl. Catal. B Environ.* **2019**, *243*, 397–414.

(32) Gu, Y.; Epling, W. S. Passive NOx Adsorber: An Overview of Catalyst Performance and Reaction Chemistry. *Appl. Catal. A Gen.* **2019**, *570*, 1–14.

(33) Kresse, G.; Hafner, J. Ab Initio Molecular Dynamics for Open-Shell Transition Metals. *Phys. Rev. B* **1993**, *48*, 13115–13118.

(34) Kresse, G.; Hafner, J. Ab Initio Molecular-Dynamics Simulation of the Liquid-Metal–Amorphous-Semiconductor Transition in Germanium. *Phys. Rev. B* **1994**, *49*, 14251–14269.

(35) Kresse, G.; Furthmüller, J. Efficiency of Ab-Initio Total Energy Calculations for Metals and Semiconductors Using a Plane-Wave Basis Set. *Comput. Mater. Sci.* **1996**.

(36) Perdew, J. P.; Burke, K.; Ernzerhof, M. Generalized Gradient Approximation Made Simple. *Phys. Rev. Lett.* **1996**, *77*, 3865–3868.

(37) Blöchl, P. E. Projector Augmented-Wave Method. *Phys. Rev. B* **1994**, *50*, 17953–17979.

(38) Kresse, G.; Joubert, D. From Ultrasoft Pseudopotentials to the Projector Augmented-Wave Method. *Phys. Rev. B* **1999**, *59*, 1758–1775.

(39) Monkhorst, H. J.; Pack, J. D. Special Points for Brillouin-Zone Integrations. *Phys. Rev. B* **1976**, *13*, 5188–5192.

(40) Grimme, S.; Ehrlich, S.; Goerigk, L. Effect of the Damping Function in Dispersion Corrected Density Functional Theory. *J. Comput. Chem.* **2011**, *32*, 1456–1465.

(41) Henkelman, G.; Jónsson, H. Improved Tangent Estimate in the Nudged Elastic Band Method for Finding Minimum Energy Paths and Saddle Points. *J. Chem. Phys.* **2000**, *113*, 9978–9985.

(42) Smith, L. J.; Davidson, A.; Cheetham, A. K. A Neutron Diffraction and Infrared Spectroscopy Study of the Acid Form of the Aluminosilicate Zeolite, Chabazite (H-SSZ-13). *Catal. Lett.* **1997**, *49*, 143–146.

(43) Szanyi, J.; Kwak, J. H.; Peden, C. H. F. The Effect of Water on the Adsorption of NO_2 in Na- and Ba-Y, FAU Zeolites: A Combined FTIR and TPD Investigation. *J. Phys. Chem. B* **2004**, *108*, 3746–3753.

(44) Yeom, Y. H.; Henao, J.; Li, M. J.; Sachtler, W. M. H.; Weitz, E. The Role of NO in the Mechanism of NO_x Reduction with Ammonia over a BaNa-Y Catalyst. *J. Catal.* **2005**, *231*, 181–193.

(45) Mochida, M.; Finlayson-Pitts, B. J. FTIR Studies of the Reaction of Gaseous NO with HNO_3 on Porous Glass: Implications for Conversion of HNO_3 to Photochemically Active NO_x in the Atmosphere. *J. Phys. Chem. A* **2000**, *104*, 9705–9711.

(46) Savara, A.; Sachtler, W. M. H.; Weitz, E. TPD of NO_2^- and NO_3^- from Na-Y: The Relative Stabilities of Nitrates and Nitrites in Low Temperature DeNOx Catalysis. *Appl. Catal. B Environ.* **2009**, *90*, 120–125.

(47) Liu, W.-G.; Goddard, W. A. First-Principles Study of the Role of Interconversion Between NO_2, N_2O_4, cis-ONO-NO_2, and trans-ONO-NO_2 in Chemical Processes. *J. Am. Chem. Soc.* **2012**, *134*, 12970–12978.

(48) Paffett, J. S. and M. T. The Adsorption of NO and Reaction of NO with O_2 on H-, NaH-, CuH-, and Cu-ZSM-5: An in Situ FTIR Investigation. *J. Catal.* **1996**, *164*, 232–245.

(49) Zhang, Y.; Peng, Y.; Li, K.; Liu, S.; Chen, J.; Li, J.; Gao, F.; Peden, C. H. F. Using Transient FTIR Spectroscopy to Probe Active Sites and Reaction Intermediates for Selective Catalytic Reduction of NO on Cu/SSZ-13 Catalysts. *ACS Catal.* **2019**, 6137–6145.

(50) Negri, C.; Hammershøi, P. S.; Janssens, T. V. W.; Beato, P.; Berlier, G.; Bordiga, S. Investigating the Low Temperature Formation of Cu^{II}-(N,O) Species on Cu-CHA Zeolites for the Selective Catalytic Reduction of NO_X. *Chem. Eur. J.* **2018**, *24*, 12044–12053.

(51) Tyrsted, C.; Borfecchia, E.; Berlier, G.; Lomachenko, K. A.; Lamberti, C.; Bordiga, S.; Vennestrøm, P. N. R.; Janssens, T. V. W.; Falsig, H.; Beato, P.; Puig-Molina, A. Nitrate-Nitrite Equilibrium in the Reaction of NO with a Cu-CHA Catalyst for NH_3-SCR. *Catal. Sci. Technol.* **2016**, *6*, 8314–8324.

(52) Janssens, T. V. W.; Falsig, H.; Lundegaard, L. F.; Vennestrøm, P. N. R.; Rasmussen, S. B.; Moses, P. G.; Giordanino, F.; Borfecchia, E.; Lomachenko, K. A.; Lamberti, C.; Bordiga, S.; Godiksen, A.; Mossin, S.; Beato, P. A Consistent Reaction Scheme for the Selective Catalytic Reduction of Nitrogen Oxides with Ammonia. *ACS Catal.* **2015**, *5*, 2832–2845.

(53) Liu, C.; Kubota, H.; Amada, T.; Kon, K.; Toyao, T.; Maeno, Z.; Ueda, K.; Ohyama, J.; Satsuma, A.; Tanigawa, T.; Tsunoji, N.; Sano, T.; Shimizu, K. In Situ Spectroscopic Studies on the Redox Cycle of NH_3−SCR over Cu−CHA Zeolites. *ChemCatChem* **2020**, *12*, 3050–3059.

(54) Brüggemann, T. C.; Przybylski, M.-D.; Balaji, S. P.; Keil, F. J. Theoretical Investigation of the Mechanism of the Selective Catalytic Reduction of Nitrogen Dioxide with Ammonia on H-Form Zeolites and the Role of Nitric and Nitrous Acids as Intermediates. *J. Phys. Chem. C* **2010**, *114*, 6567–6587.

(55) Li, J.; Li, S. New Insight into Selective Catalytic Reduction of Nitrogen Oxides by Ammonia over H-Form Zeolites: A Theoretical Study. *Phys. Chem. Chem. Phys.* **2007**, *9*, 3304–3311.

(56) Wang, X.; Qin, Q. Z.; Fan, K. Ab Initio Study on the Characterization of N2O4 Isomers. *J. Mol. Struct. THEOCHEM* **1998**, *432*, 55–62.

(57) Seifert, N. A.; Zaleski, D. P.; Fehnel, R.; Goswami, M.; Pate, B. H.; Lehmann, K. K.; Leung, H. O.; Marshall, M. D.; Stanton, J. F. The Gas-Phase Structure of the Asymmetric, Trans -Dinitrogen Tetroxide (N_2O_4), Formed by Dimerization of Nitrogen

Dioxide (NO_2), from Rotational Spectroscopy and Ab Initio Quantum Chemistry. *J. Chem. Phys.* **2017**, *146*, 134305.

(58) Paolucci, C.; Verma, A. A.; Bates, S. A.; Kispersky, V. F.; Miller, J. T.; Gounder, R.; Delgass, W. N.; Ribeiro, F. H.; Schneider, W. F. Isolation of the Copper Redox Steps in the Standard Selective Catalytic Reduction on Cu-SSZ-13. *Angew. Chem. Int. Ed.* **2014**, *53*, 11828–11833.

(59) Sun, D.; Schneider, W. F.; Adams, J. B.; Sengupta, D. Molecular Origins of Selectivity in the Reduction of NO_x by NH_3. *J. Phys. Chem. A* **2004**, *108*, 9365–9374.

(60) Mao, Y.; Wang, Z.; Wang, H. F.; Hu, P. Understanding Catalytic Reactions over Zeolites: A Density Functional Theory Study of Selective Catalytic Reduction of NOx by NH_3 over Cu-SAPO-34. *ACS Catal.* **2016**, *6*, 7882–7891.

(61) Salavati-fard, T.; Lobo, R. F.; Grabow, L. C. Linking Low and High Temperature NO Oxidation Mechanisms over Brønsted Acidic Chabazite to Dynamic Changes of the Active Site. *J. Catal.* **2020**, *389*, 195–206.

(62) Song, J.; Wang, Y.; Walter, E. D.; Washton, N. M.; Mei, D.; Kovarik, L.; Engelhard, M. H.; Prodinger, S.; Wang, Y.; Peden, C. H. F.; Gao, F. Toward Rational Design of Cu/SSZ-13 Selective Catalytic Reduction Catalysts: Implications from Atomic-Level Understanding of Hydrothermal Stability. *ACS Catal.* **2017**, *7*, 8214–8227.

(63) Luo, J.; Gao, F.; Kamasamudram, K.; Currier, N.; Peden, C. H. F.; Yezerets, A. New Insights into Cu/SSZ-13 SCR Catalyst Acidity. Part I: Nature of Acidic Sites Probed by NH_3 Titration. *J. Catal.* **2017**, *348*, 291–299.

For Table of Contents Only